

# Intelligent Reflecting Surface-aided URLLC in a Factory Automation Scenario

Hong Ren, Kezhi Wang and Cunhua Pan

## Abstract

Different from conventional wired line connections, industrial control through wireless transmission is widely regarded as a promising solution due to its reduced cost, increased long-term reliability, and enhanced reliability. However, mission-critical applications impose stringent quality of service (QoS) requirements that entail ultra-reliability low-latency communications (URLLC). The primary feature of URLLC is that the blocklength of channel codes is short, and the conventional Shannon's Capacity is not applicable. In this paper, we consider the URLLC in a factory automation (FA) scenario. Due to densely deployed equipment in FA, wireless signal are easily blocked by the obstacles. To address this issue, we propose to deploy intelligent reflecting surface (IRS) to create an alternative transmission link when the direct link is blocked, which can enhance the transmission reliability. In this paper, we focus on the performance analysis for IRS-aided URLLC-enabled communications in a FA scenario, where the direct link is blocked. Both the average data rate (ADR) and the average decoding error probability (ADEP) are derived under the case with perfect channel state information (CSI) and the case without CSI. Asymptotic analysis is performed to obtain more design insights. Extensive numerical results are provided to verify the accuracy of our derived results.

## I. INTRODUCTION

Nowadays, industry world is evolving into another new paradigm, that is the so-called fourth industrial revolution or Industrial 4.0 [1], in which more advanced manufacturing functions can be realized with the aid of industrial internet-of-things (IIoT) and artificial intelligence(AI). Hence, a more intelligent and automatic digital manufacturing system can be created. Conventionally, industrial control systems mainly rely on wired network infrastructure, where the central

H. Ren is with National Mobile Communications Research Laboratory, Southeast University, Nanjing, China. (e-mail:hren@seu.edu.cn). K. Wang is with Department of Computer and Information Sciences, Northumbria University, Newcastle, UK. (e-mail: kezhi.wang@northumbria.ac.uk). C. Pan is with the School of Electronic Engineering and Computer Science at Queen Mary University of London, U.K. (e-mail:c.pan@qmul.ac.uk).

control unit is connected to various machines through wired lines such as copper lines or optical fibers. However, there are some drawbacks by deploying wired lines. Firstly, they require expensive cables along with high installation and maintenance costs; Secondly, wired lines restrict the operation functionalities and motion ranges; Thirdly, wired lines are vulnerable to wear and tear in the applications with motion actions, and also suffer from aging; Finally, they cannot be deployed in harsh environment such as those with high temperature, high humidity and strong vibration.

As a result, the adoption of wireless networks is a promising solution to bypass all the aforementioned issues associated with wired lines. However, the industrial communications are totally different from conventional wireless communications. Instead, they require deterministic communications with the stringent quality of service requirements such as ultra reliability and low latency communications by exchanging a small amount of data such as control command data or measurement data. For typical industrial scenarios such as factory automation (FA), the maximum transmission latency is required to be kept within one millisecond, and the packet error probability should range from  $10^{-6}$ - $10^{-9}$  [2]. In addition, due to the densely deployed equipment such as mental machinery, random movement of objects (robots and trucks), and thick pillars, the wireless propagation environment in a factory is much more complex than those in home and office environment, and the wireless signals are more vulnerable to blockages, which can degrade the reliability performance.

To overcome the above hurdle, intelligent reflecting surface (IRS) is regarded as a promising solution, which has attracted considerable research interest from both academia and industry [3]–[5]. In particular, IRS is a square or circular panel that consists of a large number of passive reflecting elements, each of which can induce an independent phase shift on the impinging electromagnetic (EM) waves. Hence, by carefully designing the phase shifts of all reflecting elements, the reflected EM waves can be constructively added with the direct signal from the base station (BS) to enhance the signal power at the desired user, which can enhance the system signal-to-noise (SNR) performance. In addition, due to its passive feature, there is no need to install power-hungry hardware devices, such as power amplifier, radio frequency chains, digital-to-analogue conversion (DAC)/analogue-to-digital-to conversion (ADC), and mixers. Hence, the IRS can be fabricated with low cost, low power consumption, and light weight. Furthermore, the panel can be very thin such that it can be readily installed on walls, ceilings, street lamp, etc. As a result, the IRS is an ideal auxiliary communication device that can be integrated into the factory environment to enhance

the desired signal power when the direct signal is blocked by large machinery or other obstacles. A comprehensive survey on the research of IRS-aided wireless communications was provided in [6]–[8]. Recently, some channel modeling results were reported in [9], [10].

Most of the existing contributions on IRS focus on the transmission design for various IRS-aided wireless networks by jointly optimizing the active beamforming at the BS and the phase shift matrix at the IRS for perfect channel state information (CSI) in [11]–[25], imperfect CSI in [26]–[29], or statistical CSI in [30]–[34]. Specifically, data rate maximization problem for IRS-aided single-user case was studied in [11], [12]. For the more general IRS-aided multiuser scenario, sum power minimization, energy efficiency maximization, and sum rate maximization were investigated in [13]–[15], respectively. By deploying an IRS at the cell edge, the IRS was shown to be effective in enhancing the sum rate performance for multicell networks [17], especially for the cell-edge users. In multicast networks, the system performance is limited by the user with the worst-case channel since all the users in the same group share the same content. The IRS can be deployed to enhance the channel gain for the worst-case user, and thus significantly enhance the sum data rate performance [18]. By carefully designing the phase shifts of the IRS, the IRS was demonstrated to greatly increase the energy harvested at the energy receivers for simultaneous wireless information and power transfer (SWIPT) scenario, and thus enlarges the operation range of the wireless sensors [19]. The power minimization problem under the energy harvesting constraint was studied in [20] for an IRS-aided SWIPT communications. The IRS was also shown to be beneficial in physical layer security (PLS) networks in [21]–[24], where the IRS can be used to mitigate the information leakage to the eavesdroppers, while enhancing the received power at the desired users. The IRS was demonstrated to reduce the latency for mobile edge computing (MEC) networks in [25], where the IRS can improve the channel gain for the users that are far away from the MEC node. However, all the above-mentioned works [11]–[25] are based on the ideal assumption when the CSI can be ideally obtained at the BS. Due to the passive nature of the IRS, it is challenging to obtain the perfect CSI. Some recent contributions on channel estimation for IRS-aided communications were reported in [35]–[38], based on which robust transmission design for imperfect IRS-user CSI and for imperfect cascaded BS-IRS-user CSI were studied in [26], [27] and [28], [29], respectively. To further reduce the channel estimation overhead, the phase shifts of all reflecting elements were designed based on statistical or long-term CSI such as angle information in [30]–[33] or location information in [34].

Although extensive research efforts have been devoted to the transmission design for IRS-aided networks, only a few works studied the analytical performance in IRS-aided wireless systems [4], [39]–[50]. The performance comparison between IRS-aided systems and relaying systems were performed in [39]–[41]. For the IRS-aided single user communication system, the symbol error probability (SEP) was derived for the Rayleigh channel in [4], and the coverage probability was analyzed in [42]. The central limit theorem (CLT) was used in [4] and [42] to derive the probability density function (PDF) of signal-to-noise ratio (SNR). Then the Rayleigh channel model was extended to the more general Rician channel in [43] and Nakagami channel in [44]. The outage probability and spectral efficiency were analyzed in [45] for IRS-aided two-way networks. The exact distribution for signal-to-noise ratio (SNR) was derived in [46] for an IRS-aided millimeter wave (mmWave) communication system, where the fluctuating two-ray distribution was adopted to characterize the small-scale fading in the mmWave band. In practical system, the phase shifts can only be set with finite discrete values, which induce phase errors. Hence, recent contributions have focused on the study of the impact of the phase errors on the system performance [47]–[50]. The authors in [47] demonstrated that transmission under imperfect reflectors is equivalent to a point-to-point communication over a Nakagami fading channel. For the IRS-aided PLS networks with phase errors, secrecy outage probability and the average secrecy rate was studied in [48] for a single eavesdropper case and in [49] for the case with multiple eavesdroppers. Li *et al.* [50] quantified the capacity loss due to the impact of phase errors, and derived the minimum number of reflectors to ensure a guaranteed rate loss threshold.

All the above-mentioned contributions only focused on the traditional services with long packet, in which Shannon's Capacity is an accurate approximation of the achievable data rate. However, in a factory automation scenario with URLLC requirements, only small packets are transmitted due to the delay limit. In this case, the channel blocklength is finite, and the decoding error probability cannot approach zero for arbitrarily high SNR. Then, Shannon's Capacity can no longer be applied [51] since the law of large numbers does not hold and it cannot characterize the maximal achievable data rate with given decoding error probability. In fact, simulation results in [52] demonstrated that the delay outage probability will be underestimated if directly using Shannon's Capacity, and thus the quality of service (QoS) requirements cannot be guaranteed. In the seminal work in [53], by using normal approximation technique the authors have derived the accurate approximation of the maximal achievable rate that is valid under the short blocklength regime for the point-to-point

AWGN channel, which is a complicated function of SNR, channel blocklength, and decoding error probability. Most recently, based on the results in [53], extensive research attention has been devoted to the short packet transmission design [54]–[63] or performance analysis under the short blocklength regime [64]–[69]. However, all these contributions in [54]–[69] did not consider the IRS-aided wireless systems. To the best of our knowledge, only a few works have studied the IRS-aided URLLC networks [70], [71]. In [70], the authors proposed a novel polytope-based method to solve the overall decoding error probability minimization problem for an IRS-aided URLLC-enabled UAV system by jointly optimizing the passive beamforming, UAV location and channel blocklength. In [71], the authors studied the resource allocation problem for IRS-aided multiple-input single-output (MISO) orthogonal frequency division multiple access (OFDMA) multicell networks. However, these two papers focused on the transmission design, the analytical performance of IRS-aided systems is not yet available in the existing literature.

Against the above background, we present a comprehensive performance analysis of the end-to-end IRS-aided URLLC-enabled system in a factory automation scenario. Specifically, the main contributions are summarized as follows:

- 1) We first consider the case when CSI is not available at the BS, which is crucial for URLLC as no time resource is required for channel estimation. In this case, we derive the closed-form expression of the lower bound and the upper bound of the average data rate (ADR) under finite channel blocklength. In order to gain more design insights, we perform an asymptotic analysis of the ADR in the high SNR regime, and the results show that the ADR increases logarithmically with SNR, and will increase without bound when the number of reflecting elements approaches zero. By using the linearization technique, we also derive the approximate closed-form expression of average decoding error probability (ADEP) under finite channel blocklength. The asymptotic approximation is derived for the ADEP, which shows that the ADEP increases exponentially with the packet size.
- 2) For the case when CSI is available at the BS, the distribution of SNR is first approximated as a Gamma distribution by using the moment matching technique. We first derive the approximate ADR expression in closed-form. To obtain more design insights, some useful approximation techniques are used to simplify the derived ADR expression, based on which we quantify the performance gap between the case with perfect CSI and the case without CSI. For the ADEP, we also use the the linearization technique to derive its accurate approximate expression. The

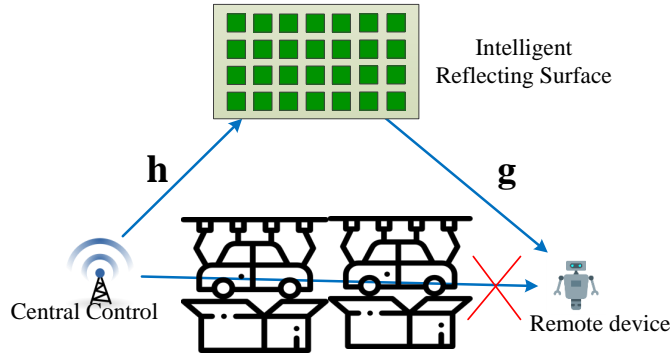


Fig. 1. Illustration of an IRS-aided automated factory scenario.

asymptotic expression is also derived to obtain more design insights. The ratio of the ADEP under the case with perfect CSI and that without CSI is derived, which demonstrates the advantages when using CSI.

- 3) Extensive numerical results obtained from Monte-Carlo simulations demonstrate the accuracy of the derived results and we also provide insightful analysis related to the number of reflecting elements, diversity order, etc.

The rest of this paper is organized as follows. Section II introduces the system model with IRS-aided point-to-point system along with the short packet theory; Section III focus on the performance analysis for the case without CSI at the BS, while Section IV is devoted to the case with CSI at the BS. Numerical results are presented in Section V to validate the accuracy of the derived results. Finally, the conclusion is drawn in Section VI.

## II. SYSTEM MODEL AND PROBLEM FORMULATION

### A. System Model

As shown in Fig. 1, we consider an IRS-aided transmission system for an automated factory scenario, where the central controller transmits command signals with short packet size to one remote device (e.g., a robot or an actuator). Due to the severe blockage caused by huge metallic machines in car manufacturing plants, the channel strength of direct links between the controller and the device is very weak and even lost. The communication link can be established via an IRS installed on the wall or the ceiling of the factory. For the sake of analysis, we assume that the controller and the device are equipped with one single antenna. The IRS is composed of  $N$  reflecting phase shifters. The complex channel vectors from the controller to the IRS and from the IRS to the device are denoted by  $\mathbf{h} \in \mathbb{C}^{N \times 1}$  and  $\mathbf{g} \in \mathbb{C}^{N \times 1}$ , respectively. Specifically, the

channel vector  $\mathbf{h}$  can be represented as  $\mathbf{h} = [h_1, \dots, h_N]^H$ , where  $h_n$  denotes the complex channel coefficient from the controller to the  $n$ -th element of the IRS that follows the distribution of  $\mathcal{CN}(0, \alpha)$ , where  $\mathcal{CN}(0, \alpha)$  means the complex Gaussian distribution with zero mean and the variance of  $\alpha$ . Similarly, we can express  $\mathbf{g}$  as  $\mathbf{g} = [g_1, \dots, g_N]^H$ , where  $g_n$  follows the distribution of  $\mathcal{CN}(0, \beta)$ . In our analysis, both  $\mathbf{h}$  and  $\mathbf{g}$  are assumed to be available at the transmitter, which provides a performance upper bound for practical applications.

Let us first denote the diagonal reflection-coefficient matrix<sup>1</sup> at the IRS by

$$\Phi = \text{diag} \{ e^{j\phi_1}, \dots, e^{j\phi_n}, \dots, e^{j\phi_N} \}, \quad (1)$$

where  $\phi_n \in [0, 2\pi]$  is the phase shift of the  $n$ -th element. By assuming that the controller transmits with fixed power  $P$ , then the received signal at the device is given by

$$r = \sqrt{P} \mathbf{g}^H \Phi \mathbf{h} x + n, \quad (2)$$

where  $x \in \mathbb{C}$  is the data information with unit power, and  $n \in \mathbb{C}$  is the noise at the user that follows zero mean and variance of  $\sigma^2$ . Then, the instantaneous SNR at the device is given by

$$\gamma = \rho |\mathbf{g}^H \Phi \mathbf{h}|^2, \quad (3)$$

where  $\rho = \frac{P}{\sigma^2}$ .

### B. Short Packet Transmission Theory

The coding rate for a communication system is defined as the ratio of the number of bits to the total number of channel uses. Shannon capacity is the largest coding rate that can be achieved such that there exists an encoder/decoder pair whose decoding error probability can approach zero when the number of channel uses is sufficiently large [72]. However, for applications in industrial factories, the number of channel uses (channel blocklength) cannot be very large due to the stringent delay requirement. As a result, the decoding error probability will not be equal to zero and has to be reconsidered [73], [74].

Let us first denote the maximum decoding error probability as  $\varepsilon$ . Then, the maximum instantaneous achievable data rate  $R$  (bit/s/Hz) [53] of the remote device can be approximated by

$$R = \log_2(1 + \gamma) - \sqrt{\frac{V(\gamma)}{M}} \frac{Q^{-1}(\varepsilon)}{\ln 2}, \quad (4)$$

<sup>1</sup> $j$  is the imaginary unit.

where  $M$  is the number of channel uses,  $Q^{-1}(\cdot)$  is the inverse function of  $Q(x) = \frac{1}{\sqrt{2\pi}} \int_x^\infty e^{-\frac{t^2}{2}} dt$ , and  $V(\gamma)$  is the channel dispersion given by  $V(\gamma) = 1 - (1 + \gamma)^{-2}$ . When the instantaneous achievable data rate  $R$  is given, the corresponding minimum decoding error probability  $\varepsilon$  is given by

$$\varepsilon = Q(f(\gamma, M, D)), \quad (5)$$

where  $f(\gamma, M, D) = \ln 2 \sqrt{\frac{M}{V(\gamma)}} (\log_2(1 + \gamma) - \frac{D}{M})$ .

In the next two sections, we analyse the average data rate (ADR) and average decoding error probability (ADEP) for two cases: channel state information (CSI) is available at the BS; CSI is not available at the BS.

### III. CSI IS NOT AVAILABLE AT THE BS

We first consider the case when CSI is not available at the BS. In this case, the phase shifts of all elements of the IRS can be set to zero, i.e.,  $\phi_n = 0, \forall n$ . Then, the phase shift matrix is given by  $\Phi = \mathbf{I}$ , and the SNR of the device is given by

$$\gamma = \rho H, \quad (6)$$

where  $H = \left| \sum_{n=1}^N g_n h_n \right|^2$  is the cascade channel gain. Based on [75], the probability density function (PDF) of  $H$  can be written as

$$f_H(x) = \frac{2x^{\frac{N-1}{2}}}{\Gamma(N)(\sqrt{\alpha\beta})^{N+1}} K_{N-1} \left( 2\sqrt{\frac{x}{\alpha\beta}} \right), \quad (7)$$

where  $\Gamma(\cdot)$  is Gamma function and  $K_n(\cdot)$  denotes the second modified Bessel function with the order  $n$ . Then, the PDF of  $\gamma$  can be calculated as follows

$$f_\gamma(x) = \frac{1}{\rho} f_H \left( \frac{x}{\rho} \right) = Ax^{\frac{N-1}{2}} K_{N-1} \left( 2\sqrt{Bx} \right), \quad (8)$$

where  $A$  and  $B$  are given by

$$A = \frac{2}{\Gamma(N)(\sqrt{\rho\alpha\beta})^{N+1}}, B = \frac{1}{\rho\alpha\beta}. \quad (9)$$

As a result, the cumulative distribution function (CDF) of  $\gamma$  can be obtained by

$$F_\gamma(x) = \int_0^x Ay^{\frac{N-1}{2}} K_{N-1} \left( 2\sqrt{By} \right) dy, \quad (10)$$

$$\stackrel{y=xz^2}{=} 2Ax^{\frac{N+1}{2}} \int_0^1 z^N K_{N-1} \left( 2\sqrt{Bxz} \right) dz, \quad (11)$$

$$\stackrel{(a)}{=} 1 - \frac{2}{(N-1)!} (Bx)^{\frac{N}{2}} K_N \left( 2\sqrt{Bx} \right), \quad (12)$$

where (a) is obtained by using Eq. (6.561.8) in [76]. Then, we study the ADR and ADEP in the following two subsections, respectively.

### A. Average Data Rate

Based on (4) and (8), the ADR can be written as

$$\bar{R} = \int_0^\infty \left( \log_2(1+x) - \sqrt{\frac{V(x)}{M}} \frac{Q^{-1}(\varepsilon)}{\ln 2} \right) f_\gamma(x) dx. \quad (13)$$

$$\begin{aligned} &= \frac{2 \left(\frac{1}{\rho}\right)^{\frac{N-1}{2}}}{\rho \Gamma(N) \sqrt{\alpha \beta}^{N+1}} \underbrace{\int_0^\infty x^{\frac{N-1}{2}} \log_2(1+x) K_{N-1} \left( 2 \sqrt{\frac{x}{\rho \alpha \beta}} \right) dx}_{U_1} \\ &\quad - \frac{2Q^{-1}(\varepsilon) \left(\frac{1}{\rho}\right)^{\frac{N-1}{2}}}{\ln 2 \cdot \rho \Gamma(N) \sqrt{\alpha \beta}^{N+1}} \underbrace{\int_0^\infty \sqrt{\frac{1 - \frac{1}{(1+x)^2}}{M}} x^{\frac{N-1}{2}} K_{N-1} \left( 2 \sqrt{\frac{x}{\rho \alpha \beta}} \right) dx}_{U_2}. \end{aligned} \quad (14)$$

Due to the complicated function of the second modified Bessel function in (14), it is challenging to obtain the closed-form expression of  $\bar{R}$ . As a result, we initially aim to obtain the lower and upper bounds of  $\bar{R}$ . The lower bound of  $\bar{R}$  is given in Lemma 1.

**Lemma 1:** The lower bound of ADR can be given by

$$\bar{R} > \frac{\left(\frac{1}{\rho}\right)^{\frac{N+1}{2}} G_{1,3}^{3,1} \left( \frac{1}{\alpha \beta \rho} \middle| \frac{1}{2}(-N-1), \frac{1}{2}(-N-1), \frac{N-1}{2} \right)}{\ln 2 \cdot \Gamma(N) \sqrt{\alpha \beta}^{N+1}} - \frac{\sqrt{\frac{1}{M}} Q^{-1}(\varepsilon)}{\ln 2}, \quad (15)$$

where  $G_{1,3}^{3,1}(\cdot)$  is Meijer G-function [76].

**Proof:** See Appendix A. ■

Similarly, the upper bound of  $\bar{R}$  can be readily obtained by ignoring the penalty term in the short packet capacity formula as

$$\bar{R} < \int_0^\infty \log_2(1+x) f_\gamma(x) dx. \quad (16)$$

After some manipulations, we have

$$\bar{R} < \hat{R} \triangleq \frac{2 \left(\frac{1}{\rho}\right)^{\frac{N-1}{2}}}{\rho(N-1)! \sqrt{\alpha \beta}^{N+1}} U_1, \quad (17)$$

where  $U_1$  is given in (A.1) in Appendix A.

To obtain more insights, we then discuss the asymptotic approximation on the ADP of the remote device which is given in the following lemma.

**Lemma 2:** When the SNR  $\gamma \rightarrow \infty$ , the ADP  $\bar{R}$  can be approximately calculated as

$$\tilde{R} = \lim_{\gamma \rightarrow \infty} \bar{R} = \frac{1}{\log(2)} \left( \sum_{k=1}^{N-1} \frac{1}{k} + \log(\alpha\beta\rho) - \frac{Q^{-1}(\varepsilon)}{\sqrt{M}} - 2\gamma_0 \right) \triangleq \bar{R}^{NCST}, \quad (18)$$

**Proof:** See Appendix B. ■

Based on the above asymptotic approximate expression of  $\bar{R}$ , we can have the following observations.

**Remark 1:** It can be observed from (18) that the ADR  $\bar{R}$  increases logarithmically with the increase of  $\alpha\beta\rho$ , and it grows unboundedly when the number of reflecting phase shifts  $N$  approaches infinity. Compared with Shannon's Capacity, the maximum instantaneous achievable data rate  $R$  under the case of short packet transmission incurs a fixed penalty term in the form of  $\frac{Q^{-1}(\varepsilon)}{\sqrt{M \log(2)}}$ , which approaches zero when the number of channel uses  $M$  approaches infinity.

### B. Average Decoding Error Probability

In this subsection, we aim to derive the average decoding error probability (ADEP) of the remote device by transmitting a packet with a fixed size of  $D$  bits. In particular, the ADEP is defined as

$$\bar{\varepsilon} = \int_0^\infty Q \left( \ln 2 \sqrt{\frac{M}{V(x)}} \left( \log_2(1+x) - \frac{D}{M} \right) \right) f_\gamma(x) dx. \quad (19)$$

Due to the complicated expression of  $Q(\cdot)$  function, it is difficult to derive the closed-form expression of (19). In the following lemma, we adopt the linearization technique to approximate  $Q(\cdot)$  and then obtain the closed-form expression of  $\bar{\varepsilon}$ .

**Lemma 3:** By adopting the linearization technique to approximate  $Q \left( \ln 2 \sqrt{\frac{M}{V(x)}} \left( \log_2(1+x) - \frac{D}{M} \right) \right)$  at point  $x = x_0$ , the expression of  $\bar{\varepsilon}$  in (19) can be approximated as

$$\bar{\varepsilon} \approx -\frac{\mu\rho^{\frac{1}{2}(-N-1)}}{\Gamma(N)(\alpha\beta)^{\frac{N+1}{2}}} U_5 + \left( \mu x_0 + \frac{1}{2} \right) \left( F_\gamma \left( \frac{1}{2\mu} + x_0 \right) - F_\gamma \left( x_0 - \frac{1}{2\mu} \right) \right) + F_\gamma \left( x_0 - \frac{1}{2\mu} \right), \quad (20)$$

where  $U_5$  is given by

$$U_5 = \frac{1}{2} \left( (N-2)! \left( f_2 \left( \frac{1}{2\mu} + x_0 \right) - f_2 \left( x_0 - \frac{1}{2\mu} \right) \right) \left( \frac{1}{\alpha\beta\rho} \right)^{\frac{1-N}{2}} \right. \\ \left. - (N-3)! \left( f_1 \left( \frac{1}{2\mu} + x_0 \right) - f_1 \left( x_0 - \frac{1}{2\mu} \right) \right) \left( \frac{1}{\alpha\beta\rho} \right)^{\frac{3-N}{2}} \right), \quad (21)$$

and  $f_1(\cdot)$  and  $f_2(\cdot)$  in (21) are given in (C.6) and (C.7) in Appendix C, respectively.

**Proof:** See Appendix C. ■

However, from Lemma 3, the accurate approximate expression of  $\bar{\epsilon}$  in (20) is complex, and cannot provide explicit design insights. To this end, we adopt a more relaxed approximation on  $Q(\cdot)$  and then obtain the asymptotic approximation expression of  $\bar{\epsilon}$  when  $\gamma \rightarrow \infty$ , which is given by the following lemma.

**Lemma 4:** A more relaxed and asymptotic approximation on  $\bar{\epsilon}$  can be approximated as

$$\bar{\epsilon} = \lim_{\gamma \rightarrow \infty} \bar{\epsilon} \approx \frac{\sqrt{2\pi} e^{\frac{1}{2M} + \frac{D}{M}}}{2\sqrt{M}(N-1)} (\alpha\beta\rho)^{-1} \triangleq \bar{\epsilon}^{NC SI}. \quad (22)$$

**Proof:** See Appendix D. ■

**Remark 2:** From (22), the ADEP  $\bar{\epsilon}^{NC SI}$  decreases with the increase of  $\alpha\beta\rho$ ,  $M$  or  $N$ , which means increasing transmit power and the number of reflecting phase shifters will enhance the reliability of the remote device. On the other hand, the ADEP increases exponentially with the packet size  $D$ .

#### IV. CSI IS AVAILABLE AT BS

In this section, we consider the case when the CSI is available at the BS. Then, the SNR of  $\gamma$  in (3) can be rewritten as

$$\gamma = \rho \left| \sum_{n=1}^N g_n h_n e^{j\phi_n} \right|^2. \quad (23)$$

With the aid of CSI at the BS, the optimal  $\phi_n$  that maximizes the instantaneous  $\gamma$  is given by

$$\phi_n^* = -\angle g_n - \angle h_n. \quad (24)$$

Then,  $\gamma$  is given as

$$\gamma = \rho \left( \sum_{n=1}^N |g_n| |h_n| \right)^2. \quad (25)$$

In the following, we derive the CDF of instantaneous SNR  $\gamma$  in (25). Define  $\xi_n = |g_n| |h_n|$  and  $\xi = \sum_{n=1}^N \xi_n$ , and we first derive the CDF and PDF of  $\xi$ . In general, it is cumbersome to derive the exact PDF and CDF of  $\xi$  and thus  $\gamma$ . To address this issue, we aim for the approximation of the CDF and PDF of  $\xi$ .

In particular, we adopt the moment matching technique as in [45], which is shown to be effective. In general, the regular Gamma distribution is widely utilized to approximate some complicated distributions by adjusting its two parameters: 1) the shape parameter  $k$ ; 2) the scale parameter  $\theta$ . The mean and variance of Gamma distribution with these two parameters are  $k\theta$  and  $k\theta^2$ ,

respectively. In the following lemma, we provide the Gamma approximation for the PDF and CDF of  $\xi_n$ .

**Lemma 5:** The distribution of  $\xi_n$  can be approximated as a Gamma distribution, and the corresponding PDF and CDF are given respectively as follows

$$f_{\xi_n}(x) \approx \frac{1}{\Gamma(k)\theta^k} x^{k-1} e^{-\frac{x}{\theta}}, F_{\xi_n}(x) \approx \frac{1}{\Gamma(k)} \gamma\left(k, \frac{x}{\theta}\right), \quad (26)$$

where  $k$  and  $\theta$  are given by

$$k = \frac{\pi^2}{16 - \pi^2}, \theta = \frac{16 - \pi^2}{4\pi} \sqrt{\alpha\beta}, \quad (27)$$

and  $\gamma(a, b)$  is the lower incomplete gamma function given by  $\gamma(a, b) = \int_0^b t^{a-1} e^{-t} dt$ .

**Proof:** See Appendix E. ■

Based on Lemma 5, we derive the approximate distribution of  $\xi$ . According to the expression of  $\xi$ , it is a sum of  $N$  i.i.d Gamma random variables with the parameters given in (27). Then, the random variable  $\xi$  follows the Gamma distribution with parameters equal to  $Nk$  and  $\theta$ . Since  $\gamma = \rho \left( \sum_{n=1}^N |g_n| |h_n| \right) = \rho \xi^2$ , we can obtain the approximate CDF of  $\gamma$  as follows

$$F_\gamma(x) \approx \frac{1}{\Gamma(Nk)} \gamma\left(Nk, \frac{1}{\theta} \sqrt{\frac{x}{\rho}}\right). \quad (28)$$

The PDF of  $\gamma$  is approximated as

$$f_\gamma(x) \approx \frac{1}{2\Gamma(Nk)} \frac{1}{\theta^{Nk} \rho^{\frac{Nk}{2}}} x^{\frac{Nk}{2}-1} e^{-\frac{1}{\theta} \sqrt{\frac{x}{\rho}}}. \quad (29)$$

Based on the above results, we proceed to derive the ADR and ADEP in the following subsections.

#### A. Average Data Rate

The average data rate (ADR) is given in the following lemma.

**Lemma 6:** ADR can be approximated as

$$\bar{R} \approx \frac{U_3}{2\rho^{\frac{kN}{2}} \theta^{kN} \Gamma(Nk)} - \frac{Q^{-1}(\varepsilon)}{\sqrt{M} \log(2)}, \quad (30)$$

where  $U_3$  is given in (F.2).

**Proof:** See Appendix F. ■

In order to gain more insights, we provide the following lemma.

**Lemma 8 :** ADR can be further approximated as

$$\bar{R} \approx \frac{2}{\log(2)} \left( \psi^{(0)}(kN) - \log \left( \frac{1}{\theta} \sqrt{\frac{1}{\rho}} \right) \right) - \frac{Q^{-1}(\varepsilon)}{\sqrt{M} \log(2)}. \quad (31)$$

By using (B.5), we have

$$\bar{R} \approx \frac{1}{\log(2)} \left( 2 \sum_{k=1}^{\frac{\pi^2 N}{16-\pi^2}-1} \frac{1}{k} + \log \left( \left( \frac{16-\pi^2}{4\pi} \right)^2 \alpha \beta \rho \right) - \frac{Q^{-1}(\varepsilon)}{\sqrt{M}} - 2\gamma_0 \right) \triangleq \bar{R}^{CSI}. \quad (32)$$

*Proof:* See Appendix G. ■

**Remark 3:** One can see from (32) that the ADR increases logarithmically with  $\rho$ ,  $\alpha$  or  $\beta$ , and increases unboundedly when  $N$  approaches infinity.

**Remark 4:** By using  $\bar{R}^{NC SI}$  in (18), we can derive the gap between the cases when CSI is available or not available as follows:

$$\bar{R}^{CSI} - \bar{R}^{NC SI} \approx \frac{1}{\log(2)} \left( \sum_{k_2=1}^{\frac{\pi^2 N_2}{16-\pi^2}-1} \frac{2}{k_2} - \sum_{k_1=1}^{N_1-1} \frac{1}{k_1} \right) + \log_2 \left( \left( \frac{16-\pi^2}{4\pi} \right)^2 \right). \quad (33)$$

If we set all the parameters to be the same for both cases e.g.,  $N_1 = N_2$ , the improvement of ADR by using CSI over that without CSI can be derived as follows:

$$\bar{R}^{CSI} - \bar{R}^{NC SI} \approx \frac{1}{\log(2)} \left( \sum_{k=1}^{N-1} \frac{1}{k} + \sum_{k=N}^{1.60994N-1} \frac{2}{k} \right) - 2.07103. \quad (34)$$

### B. Average Decoding Error Probability

In this subsection, we aim to derive the ADEP by transmitting a packet with fixed size of  $L$ . Then, the ADEP is defined as

$$\bar{\varepsilon} = \int_0^\infty Q \left( \ln 2 \sqrt{\frac{M}{V(x)}} \left( \log_2(1+x) - \frac{D}{M} \right) \right) f_\gamma(x) dx, \quad (35)$$

where  $f_\gamma(x)$  is given in (29).

Again, by using the linearization technique to approximate the Q-function, we have the following lemma.

**Lemma 8:** The closed-form expression of  $\bar{\varepsilon}$  can be derived as

$$\bar{\varepsilon} \approx \left( \mu x_0 + \frac{1}{2} \right) \left( F_\gamma \left( \frac{1}{2\mu} + x_0 \right) - F_\gamma \left( x_0 - \frac{1}{2\mu} \right) \right) + F_\gamma \left( x_0 - \frac{1}{2\mu} \right) - \frac{\mu U_6}{2\rho^{\frac{kN}{2}} \theta^{kN} \Gamma(Nk)}. \quad (36)$$

*Proof:* See Appendix H. ■

To have more insights, we derive the asymptotic expression in the following lemma.

**Lemma 9:** The asymptotic expression of ADEP is given by

$$\bar{\varepsilon} \rightarrow \frac{{}_1F_1\left(\frac{1}{4}(2 - kN); \frac{1}{2}; -\frac{1}{2}(MR_s^2)\right) 2^{1.28564kN-2} M^{-\frac{1}{4}(kN)} \Gamma\left(\frac{kN}{4}\right)}{\Gamma(kN)} (\alpha\beta\rho)^{\frac{1}{2}-kN} \triangleq \bar{\varepsilon}^{CSI} \quad (37)$$

*Proof:* See Appendix I. ■

**Remark 5:** One can see that the  $\bar{\varepsilon}$  increases asymptotically with  $(\alpha\beta\rho)^{\frac{1}{2}-kN}$ .

**Remark 6:** One can have how much performance can be approximately improved when we have CSI available at the IRS, compared with the case we have no CSI available, by using  $\bar{\varepsilon}^{NC SI}$  in (22), we have

$$\frac{\bar{\varepsilon}^{CSI}}{\bar{\varepsilon}^{NC SI}} \approx \frac{0.199471\Gamma(N)M^{\frac{1}{2}-\frac{kN}{4}}\Gamma\left(\frac{kN}{4}\right)e^{0.891137kN-\frac{1}{2M}-R_s}{}_1F_1\left(\frac{1}{4}(2 - kN); \frac{1}{2}; -\frac{1}{2}(MR_s^2)\right)}{\Gamma(N-1)\Gamma(kN)} (\alpha\beta\rho)^{1-\frac{kN}{2}}. \quad (38)$$

## V. SIMULATION RESULTS

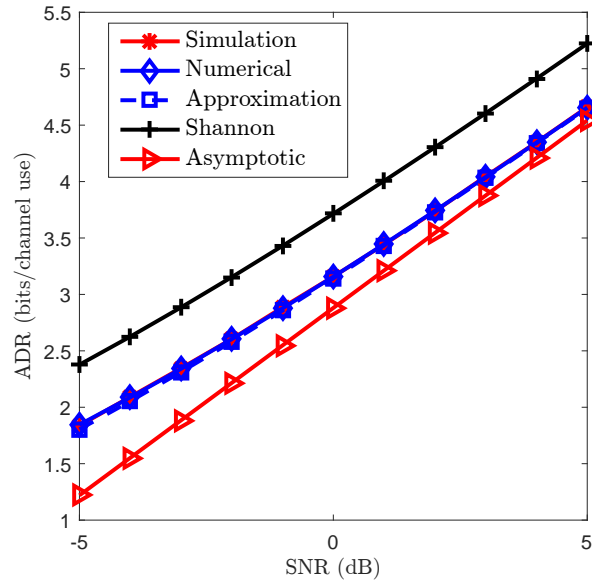
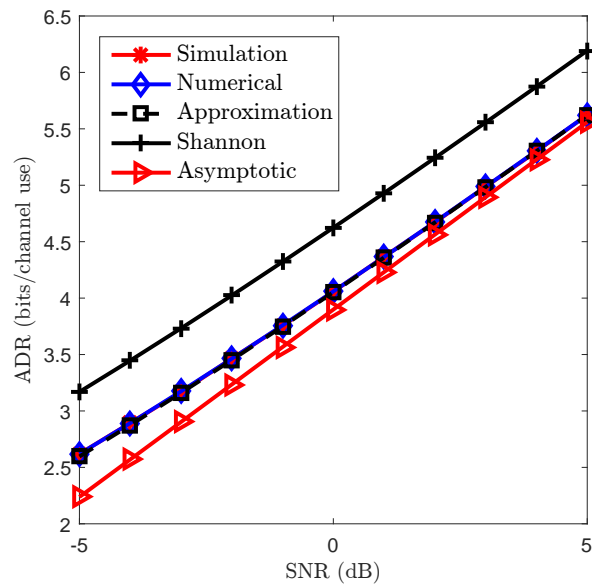
In this section, numerical results are provided to verify the accuracy of our derived results. For illustration purposes, the simulation parameters are set as follows:  $\sigma = \alpha = \beta = 1$  and  $M = 200$ . For the case of ADR,  $\varepsilon$  is set to  $\varepsilon = 10^{-8}$ , while for the case of ADEP, the number of bits is set to  $D = 100$ . Two scenarios are considered: when CSI is available or not available at the BS. The other parameters are specified in each simulation figure. The curve labelled as ‘Simulation’ is obtained by averaging over 10000 randomly and uniformly generating channels.

The curve labelled as ‘Numerical’ is obtained by using (13), (19), (F.1) and (35) in Figs. 2-5, respectively. The curve labelled as ‘Approximation’ is obtained by using (15), (20), (30) in Figs. 2-4, respectively. Additionally, the curve ‘Asymptotic’ is obtained by applying (18), (22) and (31) in Figs. 2-4, respectively. Also, the curve ‘Linerization’ is obtained by applying (C.3) and (36) in Fig. 3 and Fig. 5, respectively.

### A. When CSI is not available at the BS for ADR and ADEP

In this subsection, we verify the correctness of our derived results for the case of no CSI available at the BS.

In Fig. 2, the ADR performance is shown as a function of SNR, where two values of  $N$  are tested. The curves corresponding to ‘Numerical’, ‘Approximation’ and ‘Asymptotic’ are given in

(a)  $N = 20$ (b)  $N = 40$ Fig. 2. ADR versus SNR under  $N = 20$  and  $N = 40$  for the case when CSI is not available at the BS.

(13), (15) and (18), respectively. For comparison purposes, we also provide the curve based on Shannon's Capacity expression that can serve as the performance upper bound. It can be observed from Figs. 2 (a)-(b) that both the Numerical and Approximation have a perfect agreement with the simulation results. In addition, there is a constant gap of roughly 0.5 bits per channel use between the Shannon's capacity and the ADR, which corroborates Remark 1. The gap between Asymptotic and the simulation results becomes smaller for large values of SNR, which demonstrates the accuracy of the asymptotic results in (18). As expected, the ADR increases with SNR, and larger values of  $N$  yield high ADR due to higher passive beamforming gain brought by the IRS.

Fig. 3 depicts the ADEP versus the SNR under two different values of  $N$ . The curves corresponding to 'Numerical', 'Linerization', 'Approximation' and 'Asymptotic' are given in (19), (C.3), (20) and (22), respectively. One can observe from Figs. 3 (a)-(b) that the curves of 'Numerical', 'Linerization' and 'Approximation' coincide with the simulation results, which confirms the accuracy of our derived results and the linerization technique. It is also shown in Fig. 3 that there is a fixed gap between the simulation results and the asymptotic results. However, these two curves have the same slope, which means the asymptotic results can be used for the diversity order analysis. As expected, higher SNR produces lower ADEP, and larger values of  $N$  also yield better ADEP performance.

### B. When CSI is available at the BS for ADR and ADEP

In this subsection, we focus the case when the CSI is available at the BS.

In Fig. 4, the ADR is shown as a function of SNR for two different values of  $N$ . The curves labelled as 'Numerical', 'Approximation' and 'Asymptotic' correspond to (F.1), (30) and (31), respectively. Again, Shannon's capacity is also shown for comparison purposes. It is observed from Fig. 4 that all the curves except Shannon's capacity coincide with each other, which confirms the accuracy of our derived results. A constant gap between Shannon's capacity and ADR is observed in Fig. 4, the value of which can be calculated as  $\frac{Q^{-1}(\epsilon)}{\sqrt{M \log(2)}}$ . Also, the ADR is shown to be increasing with SNR, and larger values of  $N$  yield higher ADR. By comparing Fig. 2 with Fig. 4, for the case of  $N = 20$  and SNR = 0 dB, 3 bits per channel use and 7.4 bits per channel use are respectively achieved without CSI and with CSI. This demonstrate the necessity of obtaining CSI for transmission design.

Finally, in Fig. 5, we illustrate the ADEP versus the SNR for different values of  $N$ . The curves labelled as 'Numerical' and 'Linerization' are obtained from (35) and (36), respectively. From

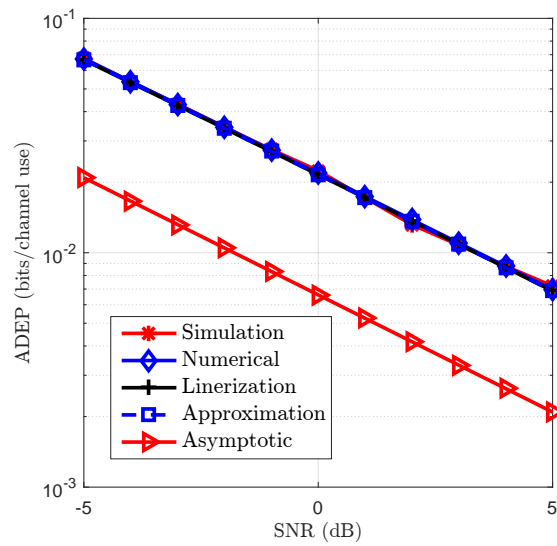
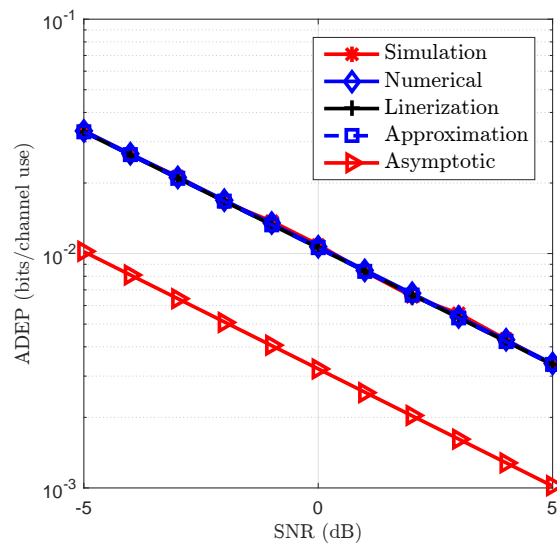
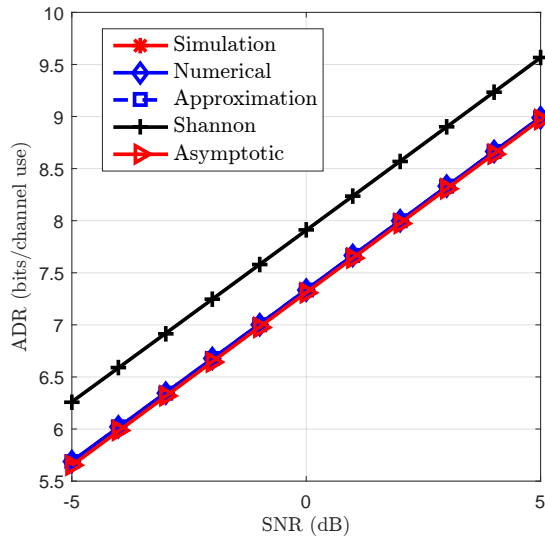
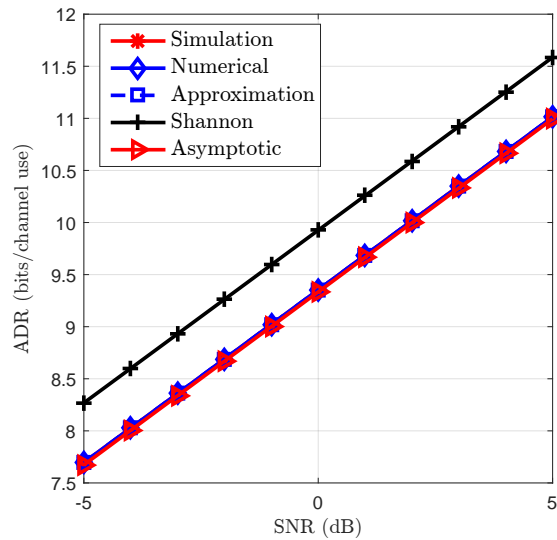
(a)  $N = 20$ (b)  $N = 40$ 

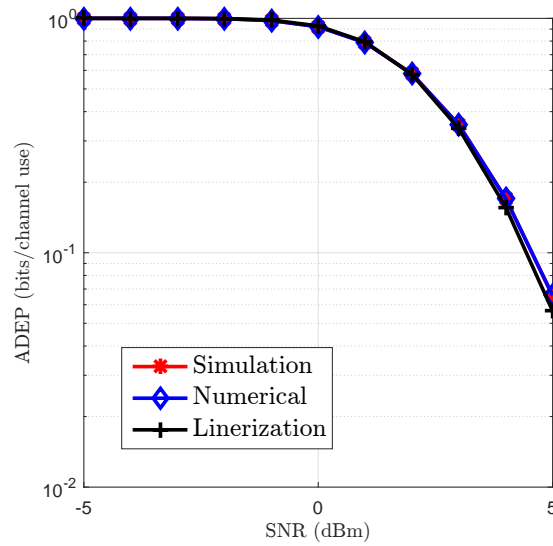
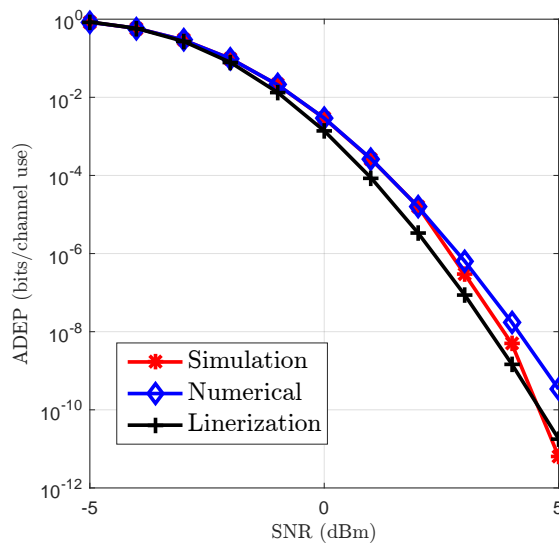
Fig. 3. ADEP versus SNR under  $N = 20$  and  $N = 40$  for the case when CSI is not available at the BS.

Fig. 5-(a) about the case of  $N = 20$ , the results obtained from ‘Numerical’ and ‘Linerization’ are consistent with the simulation results, which again verifies the accuracy of our derived results. However, for the case of  $N = 40$  in Fig. 5-(b), the Linerization curve has a little discrepancy with the simulation results. By comparing Fig. 5 with Fig. 3, significant performance gains can be obtained by using CSI over the case without CSI.

(a)  $N = 20$ (b)  $N = 40$ Fig. 4. ADR versus SNR under  $N = 20$  and  $N = 40$  for the case when CSI is available at the BS.

## VI. CONCLUSIONS

In this paper, we proposed to deploy an IRS in a FA scenario to support the URLLC. Different from the existing contributions on transmission design, this paper focused on the analytical analysis by characterizing the performance under the assistance of IRS. To this end, the performance analysis is performed under two cases: the case when no CSI is available at the BS and the case when the CSI

(a)  $N = 20$ (b)  $N = 40$ Fig. 5. ADEP versus SNR  $N = 20$  and  $N = 40$  for the case when CSI is available at the BS.

is available at the BS. For both cases, the approximate/accurate ADR and ADEP expressions were derived in closed-form. To gain more design insights, the asymptotic analysis is performed when the SNR approaches infinity. Extensive numerical results were provided to validate the accuracy of our derived results. Simulation results show that significant performance gains can be obtained by using CSI over the case without CSI.

## APPENDIX A

## PROOF OF LEMMA 1

After some manipulations [77],  $U_1$  can be rewritten as

$$U_1 = \frac{G_{1,3}^{3,1} \left( \begin{matrix} \frac{1}{\alpha\beta\rho} | & \frac{1}{2}(-N-1) \\ \frac{1}{2}(-N-1), \frac{1}{2}(-N-1), \frac{N-1}{2} \end{matrix} \right)}{2 \log(2)}. \quad (\text{A.1})$$

By using the fact that  $V(\gamma) = 1 - \frac{1}{(\gamma+1)^2} < 1$ , we can get the upper bound of  $U_2$  as follows:

$$U_2 < \int_0^\infty \sqrt{\frac{1}{M}} x^{\frac{N-1}{2}} K_{N-1} \left( 2\sqrt{\frac{x}{\alpha\beta\rho}} \right) dx = \frac{1}{2} \sqrt{\frac{1}{M}} (N-1)! (\alpha\beta\rho)^{\frac{N+1}{2}} \triangleq \hat{U}_2. \quad (\text{A.2})$$

Then, based on the results of (A.1) and (A.2), the ADR of the remote device in (13) can be obtained in (15).

## APPENDIX B

## PROOF OF LEMMA 2

When the SNR  $\gamma$  approaches infinity,  $V(\gamma)$  can be approximated as

$$V(\gamma) = 1 - \frac{1}{(\gamma+1)^2} \approx 1, \quad (\text{B.1})$$

and  $\log_2(1+\gamma)$  can be approximated as  $\log_2(\gamma+1) \approx \log_2(\gamma)$ . Then,  $U_1$  in (14) can be approximated as follows

$$\begin{aligned} U_1 &\approx \int_0^\infty x^{\frac{N-1}{2}} \log_2(x) K_{N-1} \left( 2\sqrt{\frac{x}{\rho\alpha\beta}} \right) dx \\ &= \frac{(N-1)! (\alpha\beta\rho)^{\frac{N+1}{2}} (\log(\alpha\beta\rho) + \psi^{(0)}(N) - \gamma_0)}{2 \log(2)}, \end{aligned} \quad (\text{B.2})$$

where  $\psi^n(z)$  is given for positive integer  $n$  by  $\psi^n(z) = \frac{d^n z^n \psi(z)}{dz^n}$  [78] and  $\gamma_0$  is Euler's constant with numerical value 0.577216 [79]. Similarly,  $U_2$  can be approximated as

$$U_2 \approx \frac{1}{2} \sqrt{\frac{1}{M}} (N-1)! (\alpha\beta\rho)^{\frac{N+1}{2}}. \quad (\text{B.3})$$

By substituting (B.2) into (13), the asymptotic expression of  $\bar{R}$  can be derived as

$$\lim_{\gamma \rightarrow \infty} \bar{R} = \frac{\log(\alpha\beta\rho) + \psi^{(0)}(N) - \gamma_0}{\log(2)} - \frac{Q^{-1}(\varepsilon)}{\sqrt{M} \log(2)}. \quad (\text{B.4})$$

Based on the equality [80]

$$\psi^{(0)}(N) = -\gamma_0 + \sum_{k=1}^{N-1} \frac{1}{k}, \quad (\text{B.5})$$

we can obtain the asymptotic approximation of  $\bar{R}$  as

$$\lim_{\gamma \rightarrow \infty} \bar{R} = \frac{1}{\log(2)} \left( \sum_{k=1}^{N-1} \frac{1}{k} + \log(\alpha\beta\rho) - \frac{Q^{-1}(\varepsilon)}{\sqrt{M}} - 2\gamma_0 \right). \quad (\text{B.6})$$

## APPENDIX C

## PROOF OF LEMMA 3

We adopt the linearization technique to approximate  $Q\left(\ln 2\sqrt{\frac{M}{V(x)}}\left(\log_2(1+x) - \frac{D}{M}\right)\right)$  at point  $x = x_0$  as:

$$Q\left(\ln 2\sqrt{\frac{M}{V(x)}}\left(\log_2(1+x) - \frac{D}{M}\right)\right) \approx U(x) = \begin{cases} 1, & x \leq x_0 - \frac{1}{2\mu}, \\ \frac{1}{2} - \mu(x - x_0), & x \in \left[x_0 - \frac{1}{2\mu}, x_0 + \frac{1}{2\mu}\right], \\ 0, & x \geq x_0 + \frac{1}{2\mu}, \end{cases} \quad (\text{C.1})$$

where  $\mu$  is the value of the first-order derivative of Q-function at point  $x = x_0$ , given by

$$\mu = - \left. \frac{\partial \left( Q\left(\ln 2\sqrt{\frac{M}{V(x)}}\left(\log_2(1+x) - \frac{D}{M}\right)\right) \right)}{\partial x} \right|_{x=x_0} = \sqrt{\frac{M}{2\pi \left(2^{\frac{2D}{M}} - 1\right)}}. \quad (\text{C.2})$$

In addition,  $x_0$  is given by  $x_0 = 2^{\frac{D}{M}} - 1$ .

By inserting (C.1) into (19), the ADEP can be approximated as

$$\begin{aligned} \bar{\varepsilon} \approx & F_\gamma\left(x_0 - \frac{1}{2\mu}\right) + \left(\frac{1}{2} + \mu x_0\right) \left(F_\gamma\left(x_0 + \frac{1}{2\mu}\right) - F_\gamma\left(x_0 - \frac{1}{2\mu}\right)\right) \\ & - \mu \int_{x_0 - \frac{1}{2\mu}}^{x_0 + \frac{1}{2\mu}} x f_\gamma(x) dx. \end{aligned} \quad (\text{C.3})$$

Meanwhile, by inserting (8) into (C.3), we can rewrite the above equation as

$$\begin{aligned} \bar{\varepsilon} \approx & - \frac{2\mu \left(\frac{1}{\rho}\right)^{\frac{N-1}{2}}}{\rho \left((N-1)!(\alpha\beta)^{\frac{N+1}{2}}\right)} \underbrace{\int_{x_0 - \frac{1}{2\mu}}^{x_0 + \frac{1}{2\mu}} x^{\frac{N+1}{2}} K_{N-1}\left(2\sqrt{\frac{x}{\rho\alpha\beta}}\right) dx}_{U_5} \\ & + \left(\mu x_0 + \frac{1}{2}\right) \left(F_\gamma\left(\frac{1}{2\mu} + x_0\right) - F_\gamma\left(x_0 - \frac{1}{2\mu}\right)\right) + F_\gamma\left(x_0 - \frac{1}{2\mu}\right). \end{aligned} \quad (\text{C.4})$$

The accurate expression of the second modified Bessel function  $K_n(\cdot)$  in (C.4) is complicated. To facilitate the analysis, we adopt the following simplified approximation to deal with  $K_n(\cdot)$  [8.446 of [76]],

$$K_n(z) \approx \frac{1}{2} \left( \frac{(n-1)!}{\left(\frac{z}{2}\right)^n} - \frac{(n-2)!}{\left(\frac{z}{2}\right)^{n-2}} \right). \quad (\text{C.5})$$

Furthermore, by utilizing the following two equalities,

$$f_1(x) = \int x^2 dx = \frac{x^3}{3}, \quad (\text{C.6})$$

and

$$f_2(x) = \int x dx = \frac{x^2}{2}, \quad (\text{C.7})$$

(C.4) can be transformed into (21). Hence, Lemma 3 holds.

#### APPENDIX D

##### PROOF OF LEMMA 4

According to (C.5),(8) and (19), the ADEP can be approximated as

$$\begin{aligned} \bar{\varepsilon} &\approx \frac{2\rho^{\frac{1}{2}(-N-1)}}{\Gamma(N)(\alpha\beta)^{\frac{N+1}{2}}} \\ &\int_0^\infty \frac{1}{4} x^{\frac{N-1}{2}} \operatorname{erfc} \left( \frac{\sqrt{M}(\log(1+x) - \frac{D}{M})}{\sqrt{2}} \right) \left( \frac{(N-2)!}{\left(\frac{x}{\alpha\beta\rho}\right)^{\frac{N-1}{2}}} - \frac{(N-3)!}{\left(\frac{x}{\alpha\beta\rho}\right)^{\frac{N-3}{2}}} \right) dx, \\ &= \frac{(N-2)!}{(2\Gamma(N))(\alpha\beta\rho)} \underbrace{\int_0^\infty \operatorname{erfc} \left( \frac{\sqrt{M}(\log(1+x) - \frac{D}{M})}{\sqrt{2}} \right) dx}_{U_6} \\ &\quad - \frac{(N-3)!}{(2\Gamma(N))(\alpha\beta\rho)^2} \underbrace{\int_0^\infty x \operatorname{erfc} \left( \frac{\sqrt{M}(\log(1+x) - \frac{D}{M})}{\sqrt{2}} \right) dx}_{U_7}. \end{aligned} \quad (\text{D.1})$$

Next, we use  $\operatorname{erfc}(x) \approx \exp(-x^2)$  to approximate the complementary error function in (D.1). Then, by using  $\log(1+\gamma) \approx \gamma$ ,  $U_6$  and  $U_7$  can be approximated as

$$U_6 \approx \frac{\sqrt{2\pi} e^{\frac{1}{2M} + \frac{D}{M}}}{\sqrt{M}}, \quad (\text{D.2})$$

and

$$U_7 \approx \frac{\sqrt{2\pi} e^{2(\frac{1}{M} + R_s)}}{\sqrt{M}}. \quad (\text{D.3})$$

Accordingly, the ADEP in (D.1) becomes

$$\begin{aligned} \bar{\varepsilon} &\approx \frac{(N-2)! \left( \sqrt{2\pi} e^{\frac{1}{2M} + R_s} \right)}{\sqrt{M} (2\Gamma(N)) (\alpha\beta\rho)} - \frac{(N-3)! \left( \sqrt{2\pi} e^{2(\frac{1}{M} + R_s)} \right)}{\sqrt{M} (2\Gamma(N)) (\alpha\beta\rho)^2} \\ &= \frac{\sqrt{2\pi}}{2\sqrt{M}\Gamma(N)} \left( \frac{(N-2)! e^{\frac{1}{2M} + R_s}}{\alpha\beta\rho} - \frac{(N-3)! e^{2(\frac{1}{M} + R_s)}}{(\alpha\beta\rho)^2} \right) \\ &= \frac{\sqrt{2\pi} e^{2(\frac{1}{M} + R_s)} \left( \alpha\beta(N-2)\rho e^{-\frac{3}{2M} - R_s} - 1 \right)}{2\sqrt{M}(N)(N-1)(N-2)(\alpha\beta\rho)^2} \end{aligned} \quad (\text{D.4})$$

At last, by omitting the term of  $-1$  in the numerator of equation (D.4) from above equality, (D.4) can be approximated as (22).

## APPENDIX E

## PROOF OF LEMMA 5

The first and second moments of  $\xi_n$  are given by  $E\{\xi_n\} = \frac{\pi}{4}\sqrt{\alpha\beta}$  and  $E\{\xi_n^2\} = \alpha\beta$ . Then, the mean and variance of  $\xi_n$  are given by  $\frac{\pi}{4}\sqrt{\alpha\beta}$  and  $\frac{16-\pi^2}{16}\alpha\beta$ , respectively. Next, we construct a regular Gamma distribution with the same mean and variance:

$$k\theta = \frac{\pi}{4}\sqrt{\alpha\beta}, k\theta^2 = \frac{16-\pi^2}{16}\alpha\beta. \quad (\text{E.1})$$

By solving the above equations, we can obtain the values of  $k$  and  $\theta$  in (27).

## APPENDIX F

## PROOF OF LEMMA 6

By using the approximate PDF of  $\gamma$  in (29),  $\bar{R}$  can be approximated as

$$\begin{aligned} \bar{R} &\approx \int_0^\infty \left( \log_2(1+x) - \frac{Q^{-1}(\varepsilon)}{\ln 2} \sqrt{\frac{V(x)}{M}} \right) f_\gamma(x) dx \\ &= \frac{1}{2\rho^{\frac{kN}{2}} \theta^{kN} \Gamma(Nk)} \underbrace{\int_0^\infty \log_2(1+x) \left( x^{\frac{kN}{2}-1} \exp\left(-\frac{1}{\theta} \sqrt{\frac{x}{\rho}}\right) \right) dx}_{U_3} - \\ &\quad \frac{Q^{-1}(\varepsilon)}{2\log(2)\rho^{\frac{kN}{2}} \theta^{kN} \Gamma(Nk)} \underbrace{\int_0^\infty \sqrt{\frac{1-\frac{1}{(1+x)^2}}{M}} \left( x^{\frac{kN}{2}-1} \exp\left(-\frac{1}{\theta} \sqrt{\frac{x}{\rho}}\right) \right) dx}_{U_4}. \end{aligned} \quad (\text{F.1})$$

Then, one can have

$$\begin{aligned} U_3 &= \int_0^\infty \log_2(1+x) \left( x^{\frac{kN}{2}-1} \exp\left(-\frac{1}{\theta} \sqrt{\frac{x}{\rho}}\right) \right) dx \\ &= \frac{2\rho^{\frac{kN}{2}-1} \theta^{kN-2} \Gamma(kN) {}_2F_3\left(1, 1; 2, \frac{3}{2} - \frac{kN}{2}, 2 - \frac{kN}{2}; -\frac{1}{4\rho\theta^2}\right)}{\log(2)(kN-2)(kN-1)} - \\ &\quad \frac{2\pi\sqrt{\frac{1}{\rho}} \sec\left(\frac{\pi kN}{2}\right) {}_1F_2\left(\frac{kN}{2} + \frac{1}{2}; \frac{3}{2}, \frac{kN}{2} + \frac{3}{2}; -\frac{1}{4\rho\theta^2}\right)}{\log(2)(kN\theta + \theta)} + \\ &\quad \frac{2\pi \csc\left(\frac{\pi kN}{2}\right) {}_1F_2\left(\frac{kN}{2}; \frac{1}{2}, \frac{kN}{2} + 1; -\frac{1}{4\rho\theta^2}\right)}{kN \log(2)} - \frac{4\Gamma(kN) \log\left(\frac{1}{\theta} \sqrt{\frac{1}{\rho}}\right) \left(\frac{1}{\theta} \sqrt{\frac{1}{\rho}}\right)^{-kN}}{\log(2)} \\ &\quad + \frac{4\Gamma(kN) \psi^{(0)}(kN) \left(\frac{1}{\theta} \sqrt{\frac{1}{\rho}}\right)^{-kN}}{\log(2)}, \end{aligned} \quad (\text{F.2})$$

where  $\psi^{(0)}(n)$  is the logarithmic Gamma function and  ${}_pF_q(\cdot; \cdot; \cdot)$  is the generalized hypergeometric functions [76].

By using  $V(\gamma) = 1 - \frac{1}{(\gamma+1)^2} \approx 1$ , one can have

$$U_4 \approx \int_0^\infty \sqrt{\frac{1}{M}} x^{\frac{kN}{2}-1} e^{-\frac{\sqrt{x}}{\theta}} dx = 2\sqrt{\frac{1}{M}} \Gamma(kN) \left(\frac{1}{\theta} \sqrt{\frac{1}{\rho}}\right)^{-kN} \quad (\text{F.3})$$

Then,  $\bar{R}$  in (F.1) can be approximated as

$$\bar{R} = \frac{U_3}{2\rho^{\frac{kN}{2}} \theta^{kN} \Gamma(Nk)} - \frac{U_4 Q^{-1}(\varepsilon)}{2 \log(2) \rho^{\frac{kN}{2}} \theta^{kN} \Gamma(Nk)} \quad (\text{F.4})$$

which can be further simplified as (30).

## APPENDIX G

### PROOF OF LEMMA 7

By using  $\log(1 + \gamma) \approx \gamma$  when  $\gamma \rightarrow \infty$ ,  $U_3$  in (F.1) can be further simplified as

$$\begin{aligned} U_3 &\approx \int_0^\infty \log_2(\gamma) \left( \gamma^{\frac{kN}{2}-1} \exp\left(-\frac{1}{\theta} \sqrt{\frac{\gamma}{\rho}}\right) \right) d\gamma \\ &= \frac{4\Gamma(kN) \left(\frac{1}{\theta} \sqrt{\frac{1}{\rho}}\right)^{-kN} \left( \psi^{(0)}(kN) - \log\left(\frac{1}{\theta} \sqrt{\frac{1}{\rho}}\right) \right)}{\log(2)} \end{aligned} \quad (\text{G.1})$$

Then, we can have  $\bar{R}$  in (31).

## APPENDIX H

### PROOF OF LEMMA 8

Similar to the proof of Lemma 3,  $\bar{\varepsilon}$  can be approximated as

$$\begin{aligned} \bar{\varepsilon} &\approx F_\gamma\left(x_0 - \frac{1}{2\mu}\right) + \left(\frac{1}{2} + \mu x_0\right) \left( F_\gamma\left(x_0 + \frac{1}{2\mu}\right) - F_\gamma\left(x_0 - \frac{1}{2\mu}\right) \right) - \mu \int_{x_0 - \frac{1}{2\mu}}^{x_0 + \frac{1}{2\mu}} x f_\gamma(x) dx \\ &= -\frac{\mu}{2\rho^{\frac{kN}{2}} \theta^{kN} \Gamma(Nk)} \underbrace{\int_{x_0 - \frac{1}{2\mu}}^{x_0 + \frac{1}{2\mu}} x^{\frac{kN}{2}} \exp\left(-\frac{1}{\theta} \sqrt{\frac{x}{\rho}}\right) dx}_{U_6} \\ &\quad + \left(\mu x_0 + \frac{1}{2}\right) \left( F_\gamma\left(\frac{1}{2\mu} + x_0\right) - F_\gamma\left(x_0 - \frac{1}{2\mu}\right) \right) + F_\gamma\left(x_0 - \frac{1}{2\mu}\right). \end{aligned} \quad (\text{H.1})$$

By using

$$\int \gamma^{\frac{kN}{2}} \exp\left(-\frac{1}{\theta} \sqrt{\frac{\gamma}{\rho}}\right) d\gamma = -2\rho^{\frac{kN}{2}+1} \theta^{kN+2} \Gamma\left(kN + 2, \frac{1}{\theta} \sqrt{\frac{\gamma}{\rho}}\right) \triangleq f_3(\gamma), \quad (\text{H.2})$$

one can have

$$U_6 = f_3\left(x_0 + \frac{1}{2\mu}\right) - f_3\left(x_0 - \frac{1}{2\mu}\right). \quad (\text{H.3})$$

Then, by using  $U_6$  in (H.3),  $\bar{\varepsilon}$  in (H.1) can be written in (36).

APPENDIX I  
PROOF OF LEMMA 9

By using (35), one can have

$$\bar{\varepsilon} \approx \frac{\rho^{-\frac{1}{2}(kN)}\theta^{-kN}}{4\Gamma(kN)} \int_0^\infty x^{\frac{kN}{2}-1} e^{-\frac{1}{\theta}\sqrt{\frac{x}{\rho}}} \operatorname{erfc}\left(\frac{\sqrt{M}(\log(1+x) - R_s)}{\sqrt{2}}\right) dx. \quad (\text{I.1})$$

By using  $\operatorname{erfc}(x) \approx \exp(-x^2)$ , (I.1) can be approximated as

$$\bar{\varepsilon} \approx \frac{\rho^{-\frac{1}{2}(kN)}\theta^{-kN}}{4\Gamma(kN)} \int_0^\infty x^{\frac{kN}{2}-1} e^{-\frac{1}{\theta}\sqrt{\frac{x}{\rho}}} e^{-\frac{1}{2}(M(\log(1+x)-R_s)^2)} dx. \quad (\text{I.2})$$

When  $\rho \gg 1$ , one can have

$$e^{-\frac{1}{\theta}\sqrt{\frac{x}{\rho}}} \approx 1. \quad (\text{I.3})$$

Then, (I.2) becomes

$$\bar{\varepsilon} \approx \frac{\rho^{-\frac{1}{2}(kN)}\theta^{-kN}}{4\Gamma(kN)} \int_0^\infty x^{\frac{kN}{2}-1} e^{-\frac{1}{2}(M(\log(1+x)-R_s)^2)} dx. \quad (\text{I.4})$$

By using  $\log_2(1+\gamma) \approx \gamma$  when  $\rho \gg 1$ , we can have

$$\bar{\varepsilon} \approx \frac{\rho^{-\frac{1}{2}(kN)}\theta^{-kN}}{4\Gamma(kN)} \int_0^\infty x^{\frac{kN}{2}-1} e^{-\frac{1}{2}(M(x-R_s)^2)} dx. \quad (\text{I.5})$$

Then, by using

$$\begin{aligned} & \int_0^\infty x^{\frac{kN}{2}-1} e^{-\frac{1}{2}(M(x-R_s)^2)} dx \\ &= 2^{\frac{1}{4}(kN-6)} M^{-\frac{1}{4}(kN)} \left( \sqrt{2}\Gamma\left(\frac{kN}{4}\right) {}_1F_1\left(\frac{1}{4}(2-kN); \frac{1}{2}; -\frac{1}{2}(MR_s^2)\right) \right. \\ & \quad \left. + 2\sqrt{M}R_s\Gamma\left(\frac{1}{4}(kN+2)\right) {}_1F_1\left(1-\frac{kN}{4}; \frac{3}{2}; -\frac{1}{2}(MR_s^2)\right) \right), \end{aligned} \quad (\text{I.6})$$

$\bar{\varepsilon}$  in (I.5) becomes

$$\begin{aligned} \bar{\varepsilon} \approx & \frac{\left(2^{\frac{kN}{4}-\frac{7}{2}} M^{-\frac{1}{4}(kN)} \rho^{-\frac{1}{2}(kN)} \theta^{-kN}\right)}{\Gamma(kN)} \left( \sqrt{2}\Gamma\left(\frac{kN}{4}\right) {}_1F_1\left(\frac{1}{4}(2-kN); \frac{1}{2}; -\frac{1}{2}(MR_s^2)\right) \right. \\ & \left. + 2\sqrt{M}R_s\Gamma\left(\frac{1}{4}(kN+2)\right) {}_1F_1\left(1-\frac{kN}{4}; \frac{3}{2}; -\frac{1}{2}(MR_s^2)\right) \right). \end{aligned} \quad (\text{I.7})$$

From our simulations, we also have

$$\begin{aligned} & \sqrt{2}\Gamma\left(\frac{kN}{4}\right) {}_1F_1\left(\frac{1}{4}(2-kN); \frac{1}{2}; -\frac{1}{2}(MR_s^2)\right) \\ & \approx 2\sqrt{M}R_s\Gamma\left(\frac{1}{4}(kN+2)\right) {}_1F_1\left(1-\frac{kN}{4}; \frac{3}{2}; -\frac{1}{2}(MR_s^2)\right). \end{aligned} \quad (\text{I.8})$$

Also, by using  $\pi = 3.1415926$ ,  $\bar{\varepsilon}$  in (I.7) can be further approximated as (37).

## REFERENCES

- [1] K. Schwab, *The fourth industrial revolution*. Currency, 2017.
- [2] Z. Pang, M. Luvisotto, and D. Dzung, "Wireless high-performance communications: The challenges and opportunities of a new target," *IEEE Industrial Electronics Magazine*, vol. 11, no. 3, pp. 20–25, 2017.
- [3] Q. Wu and R. Zhang, "Towards smart and reconfigurable environment: Intelligent reflecting surface aided wireless network," *IEEE Communications Magazine*, vol. 58, no. 1, pp. 106–112, 2019.
- [4] E. Basar, M. Di Renzo, J. De Rosny, M. Debbah, M. Alouini, and R. Zhang, "Wireless communications through reconfigurable intelligent surfaces," *IEEE Access*, vol. 7, pp. 116 753–116 773, 2019.
- [5] C. Pan, H. Ren, K. Wang, J. F. Kolb, M. ElKashlan, M. Chen, M. Renzo, Y. Hao, J. Wang, A. Swindlehurst *et al.*, "Reconfigurable intelligent surfaces for 6G and beyond: Principles, applications, and research directions." [Online]. Available: <https://arxiv.org/abs/2011.04300>
- [6] S. Gong, X. Lu, D. T. Hoang, D. Niyato, L. Shu, D. I. Kim, and Y. C. Liang, "Toward smart wireless communications via intelligent reflecting surfaces: A contemporary survey," *IEEE Communications Surveys Tutorials*, vol. 22, no. 4, pp. 2283–2314, 2020.
- [7] M. Di Renzo, A. Zappone, M. Debbah, M. S. Alouini, C. Yuen, J. de Rosny, and S. Tretyakov, "Smart radio environments empowered by reconfigurable intelligent surfaces: How it works, state of research, and the road ahead," *IEEE Journal on Selected Areas in Communications*, vol. 38, no. 11, pp. 2450–2525, 2020.
- [8] Q. Wu, S. Zhang, B. Zheng, C. You, and R. Zhang, "Intelligent reflecting surface aided wireless communications: A tutorial," *IEEE Transactions on Communications*, pp. 1–1, 2021.
- [9] O. Ozdogan, E. Bjornson, and E. G. Larsson, "Intelligent reflecting surfaces: Physics, propagation, and pathloss modeling," *IEEE Wireless Communications Letters*, vol. 9, no. 5, pp. 581–585, 2020.
- [10] W. Tang, M. Z. Chen, X. Chen, J. Y. Dai, Y. Han, M. Di Renzo, Y. Zeng, S. Jin, Q. Cheng, and T. J. Cui, "Wireless communications with reconfigurable intelligent surface: Path loss modeling and experimental measurement," *IEEE Transactions on Wireless Communications*, vol. 20, no. 1, pp. 421–439, 2021.
- [11] X. Yu, D. Xu, and R. Schober, "MISO wireless communication systems via intelligent reflecting surfaces : (invited paper)," in *2019 IEEE/CIC International Conference on Communications in China (ICCC)*, 2019, pp. 735–740.
- [12] S. Zhang and R. Zhang, "Capacity characterization for intelligent reflecting surface aided mimo communication," *IEEE Journal on Selected Areas in Communications*, vol. 38, no. 8, pp. 1823–1838, 2020.
- [13] Q. Wu and R. Zhang, "Intelligent reflecting surface enhanced wireless network via joint active and passive beamforming," *IEEE Transactions on Wireless Communications*, vol. 18, no. 11, pp. 5394–5409, 2019.
- [14] C. Huang, A. Zappone, G. C. Alexandropoulos, M. Debbah, and C. Yuen, "Reconfigurable intelligent surfaces for energy efficiency in wireless communication," *IEEE Transactions on Wireless Communications*, vol. 18, no. 8, pp. 4157–4170, 2019.
- [15] H. Guo, Y. Liang, J. Chen, and E. G. Larsson, "Weighted sum-rate maximization for reconfigurable intelligent surface aided wireless networks," *IEEE Transactions on Wireless Communications*, vol. 19, no. 5, pp. 3064–3076, 2020.
- [16] B. Di, H. Zhang, L. Song, Y. Li, Z. Han, and H. V. Poor, "Hybrid beamforming for reconfigurable intelligent surface based multi-user communications: Achievable rates with limited discrete phase shifts," *IEEE Journal on Selected Areas in Communications*, vol. 38, no. 8, pp. 1809–1822, 2020.
- [17] C. Pan, H. Ren, K. Wang, W. Xu, M. ElKashlan, A. Nallanathan, and L. Hanzo, "Multicell MIMO communications relying on intelligent reflecting surfaces," *IEEE Transactions on Wireless Communications*, vol. 19, no. 8, pp. 5218–5233, 2020.
- [18] G. Zhou, C. Pan, H. Ren, K. Wang, and A. Nallanathan, "Intelligent reflecting surface aided multigroup multicast MISO communication systems," *IEEE Transactions on Signal Processing*, vol. 68, pp. 3236–3251, 2020.

- [19] C. Pan, H. Ren, K. Wang, M. ElKashlan, A. Nallanathan, J. Wang, and L. Hanzo, "Intelligent reflecting surface aided MIMO broadcasting for simultaneous wireless information and power transfer," *IEEE Journal on Selected Areas in Communications*, vol. 38, no. 8, pp. 1719–1734, 2020.
- [20] Q. Wu and R. Zhang, "Weighted sum power maximization for intelligent reflecting surface aided SWIPT," *IEEE Wireless Communications Letters*, vol. 9, no. 5, pp. 586–590, 2020.
- [21] M. Cui, G. Zhang, and R. Zhang, "Secure wireless communication via intelligent reflecting surface," *IEEE Wireless Communications Letters*, vol. 8, no. 5, pp. 1410–1414, 2019.
- [22] Z. Chu, W. Hao, P. Xiao, and J. Shi, "Intelligent reflecting surface aided multi-antenna secure transmission," *IEEE Wireless Communications Letters*, vol. 9, no. 1, pp. 108–112, 2020.
- [23] L. Dong and H. Wang, "Secure MIMO transmission via intelligent reflecting surface," *IEEE Wireless Communications Letters*, vol. 9, no. 6, pp. 787–790, 2020.
- [24] S. Hong, C. Pan, H. Ren, K. Wang, and A. Nallanathan, "Artificial-noise-aided secure MIMO wireless communications via intelligent reflecting surface," *IEEE Transactions on Communications*, vol. 68, no. 12, pp. 7851–7866, 2020.
- [25] T. Bai, C. Pan, Y. Deng, M. ElKashlan, A. Nallanathan, and L. Hanzo, "Latency minimization for intelligent reflecting surface aided mobile edge computing," *IEEE Journal on Selected Areas in Communications*, vol. 38, no. 11, pp. 2666–2682, 2020.
- [26] G. Zhou, C. Pan, H. Ren, K. Wang, M. D. Renzo, and A. Nallanathan, "Robust beamforming design for intelligent reflecting surface aided MISO communication systems," *IEEE Wireless Communications Letters*, vol. 9, no. 10, pp. 1658–1662, 2020.
- [27] X. Yu, D. Xu, Y. Sun, D. W. K. Ng, and R. Schober, "Robust and secure wireless communications via intelligent reflecting surfaces," *IEEE Journal on Selected Areas in Communications*, vol. 38, no. 11, pp. 2637–2652, 2020.
- [28] G. Zhou, C. Pan, H. Ren, K. Wang, and A. Nallanathan, "A framework of robust transmission design for IRS-aided MISO communications with imperfect cascaded channels," *IEEE Transactions on Signal Processing*, vol. 68, pp. 5092–5106, 2020.
- [29] S. Hong, C. Pan, H. Ren, K. Wang, K. K. Chai, and A. Nallanathan, "Robust transmission design for intelligent reflecting surface aided secure communication systems with imperfect cascaded CSI," *IEEE Transactions on Wireless Communications*, pp. 1–1, 2020.
- [30] Y. Han, W. Tang, S. Jin, C. Wen, and X. Ma, "Large intelligent surface-assisted wireless communication exploiting statistical CSI," *IEEE Transactions on Vehicular Technology*, vol. 68, no. 8, pp. 8238–8242, 2019.
- [31] Y. Jia, C. Ye, and Y. Cui, "Analysis and optimization of an intelligent reflecting surface-assisted system with interference," *IEEE Transactions on Wireless Communications*, vol. 19, no. 12, pp. 8068–8082, 2020.
- [32] Z. Peng, T. Li, C. Pan, H. Ren, W. Xu, and M. D. Renzo, "Analysis and optimization for ris-aided multi-pair communications relying on statistical CSI." [Online]. Available: <https://arxiv.org/abs/2007.11704>
- [33] K. Zhi, C. Pan, H. Ren, and K. Wang, "Statistical CSI-based design for reconfigurable intelligent surface-aided massive MIMO systems with direct links." [Online]. Available: <https://arxiv.org/abs/2012.07030>
- [34] X. Hu, C. Zhong, Y. Zhang, X. Chen, and Z. Zhang, "Location information aided multiple intelligent reflecting surface systems," *IEEE Transactions on Communications*, vol. 68, no. 12, pp. 7948–7962, 2020.
- [35] Z. He and X. Yuan, "Cascaded channel estimation for large intelligent metasurface assisted massive MIMO," *IEEE Wireless Communications Letters*, vol. 9, no. 2, pp. 210–214, 2020.
- [36] B. Zheng and R. Zhang, "Intelligent reflecting surface-enhanced OFDM: Channel estimation and reflection optimization," *IEEE Wireless Communications Letters*, vol. 9, no. 4, pp. 518–522, 2020.
- [37] C. You, B. Zheng, and R. Zhang, "Channel estimation and passive beamforming for intelligent reflecting surface: Discrete phase shift and progressive refinement," *IEEE Journal on Selected Areas in Communications*, vol. 38, no. 11, pp. 2604–2620, 2020.

- [38] Z. Wang, L. Liu, and S. Cui, "Channel estimation for intelligent reflecting surface assisted multiuser communications: Framework, algorithms, and analysis," *IEEE Transactions on Wireless Communications*, vol. 19, no. 10, pp. 6607–6620, 2020.
- [39] E. Bjornson, O. Ozdogan, and E. G. Larsson, "Intelligent reflecting surface versus decode-and-forward: How large surfaces are needed to beat relaying?" *IEEE Wireless Communications Letters*, vol. 9, no. 2, pp. 244–248, 2020.
- [40] A. A. Boulogeorgos and A. Alexiou, "Performance analysis of reconfigurable intelligent surface-assisted wireless systems and comparison with relaying," *IEEE Access*, vol. 8, pp. 94 463–94 483, 2020.
- [41] M. Di Renzo, K. Ntontin, J. Song, F. H. Danufane, X. Qian, F. Lazarakis, J. De Rosny, D. T. Phan-Huy, O. Simeone, R. Zhang, M. Debbah, G. Lerosey, M. Fink, S. Tretyakov, and S. Shamai, "Reconfigurable intelligent surfaces vs. relaying: Differences, similarities, and performance comparison," *IEEE Open Journal of the Communications Society*, vol. 1, pp. 798–807, 2020.
- [42] L. Yang, Y. Yang, M. O. Hasna, and M. S. Alouini, "Coverage, probability of SNR gain, and DOR analysis of RIS-aided communication systems," *IEEE Wireless Communications Letters*, vol. 9, no. 8, pp. 1268–1272, 2020.
- [43] Q. Tao, J. Wang, and C. Zhong, "Performance analysis of intelligent reflecting surface aided communication systems," *IEEE Communications Letters*, vol. 24, no. 11, pp. 2464–2468, 2020.
- [44] H. Ibrahim, H. Tabassum, and U. T. Nguyen, "Exact coverage analysis of intelligent reflecting surfaces with Nakagami-m channels," *IEEE Transactions on Vehicular Technology*, pp. 1–1, 2021.
- [45] S. Atapattu, R. Fan, P. Dharmawansa, G. Wang, J. Evans, and T. A. Tsiftsis, "Reconfigurable intelligent surface assisted two-way communications: Performance analysis and optimization," *IEEE Transactions on Communications*, vol. 68, no. 10, pp. 6552–6567, 2020.
- [46] H. Du, J. Zhang, J. Cheng, and B. Ai, "Millimeter wave communications with reconfigurable intelligent surfaces: Performance analysis and optimization," *IEEE Transactions on Communications*, pp. 1–1, 2021.
- [47] M. Badiu and J. P. Coon, "Communication through a large reflecting surface with phase errors," *IEEE Wireless Communications Letters*, vol. 9, no. 2, pp. 184–188, 2020.
- [48] J. D. V. Snchez, P. Ramirez-Espinosa, and F. J. Lpez-Martnez, "Physical layer security of large reflecting surface aided communications with phase errors," *IEEE Wireless Communications Letters*, pp. 1–1, 2020.
- [49] P. Xu, G. Chen, G. Pan, and M. Di Renzo, "Ergodic secrecy rate of RIS-assisted communication systems in the presence of discrete phase shifts and multiple eavesdroppers," *IEEE Wireless Communications Letters*, pp. 1–1, 2020.
- [50] D. Li, "Ergodic capacity of intelligent reflecting surface-assisted communication systems with phase errors," *IEEE Communications Letters*, vol. 24, no. 8, pp. 1646–1650, 2020.
- [51] G. Durisi, T. Koch, and P. Popovski, "Toward massive, ultrareliable, and low-latency wireless communication with short packets," *Proceedings of the IEEE*, vol. 104, no. 9, pp. 1711–1726, 2016.
- [52] S. Schiessl, J. Gross, and H. Al-Zubaidy, "Delay analysis for wireless fading channels with finite blocklength channel coding," in *Proceedings of the 18th ACM International Conference on Modeling, Analysis and Simulation of Wireless and Mobile Systems*, 2015, pp. 13–22.
- [53] Y. Polyanskiy, H. V. Poor, and S. Verdú, "Channel coding rate in the finite blocklength regime," *IEEE Transactions on Information Theory*, vol. 56, no. 5, pp. 2307–2359, 2010.
- [54] X. Sun, S. Yan, N. Yang, Z. Ding, C. Shen, and Z. Zhong, "Short-packet downlink transmission with non-orthogonal multiple access," *IEEE Transactions on Wireless Communications*, vol. 17, no. 7, pp. 4550–4564, 2018.
- [55] W. R. Ghanem, V. Jamali, Y. Sun, and R. Schober, "Resource allocation for multi-user downlink URLLC-OFDMA systems," in *2019 IEEE International Conference on Communications Workshops (ICC Workshops)*, 2019, pp. 1–6.

- [56] C. She, C. Yang, and T. Q. S. Quek, "Joint uplink and downlink resource configuration for ultra-reliable and low-latency communications," *IEEE Transactions on Communications*, vol. 66, no. 5, pp. 2266–2280, 2018.
- [57] S. Han, X. Xu, Z. Liu, P. Xiao, K. Moessner, X. Tao, and P. Zhang, "Energy-efficient short packet communications for uplink NOMA-based massive MTC networks," *IEEE Transactions on Vehicular Technology*, vol. 68, no. 12, pp. 12 066–12 078, 2019.
- [58] A. Avranas, M. Kountouris, and P. Ciblat, "Energy-latency tradeoff in ultra-reliable low-latency communication with retransmissions," *IEEE Journal on Selected Areas in Communications*, vol. 36, no. 11, pp. 2475–2485, 2018.
- [59] J. Chen, L. Zhang, Y. Liang, X. Kang, and R. Zhang, "Resource allocation for wireless-powered IoT networks with short packet communication," *IEEE Transactions on Wireless Communications*, vol. 18, no. 2, pp. 1447–1461, 2019.
- [60] Y. Hu, Y. Zhu, M. C. Gursoy, and A. Schmeink, "SWIPT-enabled relaying in IoT networks operating with finite blocklength codes," *IEEE Journal on Selected Areas in Communications*, vol. 37, no. 1, pp. 74–88, 2019.
- [61] H. Ren, C. Pan, Y. Deng, M. ElKashlan, and A. Nallanathan, "Joint power and blocklength optimization for URLLC in a factory automation scenario," *IEEE Transactions on Wireless Communications*, vol. 19, no. 3, pp. 1786–1801, 2020.
- [62] —, "Joint pilot and payload power allocation for massive-MIMO-enabled URLLC IIoT networks," *IEEE Journal on Selected Areas in Communications*, vol. 38, no. 5, pp. 816–830, 2020.
- [63] B. Makki, T. Svensson, and M. Zorzi, "Finite block-length analysis of the incremental redundancy HARQ," *IEEE Wireless Communications Letters*, vol. 3, no. 5, pp. 529–532, 2014.
- [64] O. L. A. Lpez, H. Alves, R. D. Souza, and E. M. G. Fernndez, "Ultrareliable short-packet communications with wireless energy transfer," *IEEE Signal Processing Letters*, vol. 24, no. 4, pp. 387–391, 2017.
- [65] J. Zheng, Q. Zhang, and J. Qin, "Average block error rate of downlink NOMA short-packet communication systems in nakagami-  $m$  fading channels," *IEEE Communications Letters*, vol. 23, no. 10, pp. 1712–1716, 2019.
- [66] —, "Average block error rate of downlink noma short-packet communication systems in nakagami-  $m$  fading channels," *IEEE Communications Letters*, vol. 23, no. 10, pp. 1712–1716, 2019.
- [67] S. Schiessl, H. Al-Zubaidy, M. Skoglund, and J. Gross, "Delay performance of wireless communications with imperfect CSI and finite-length coding," *IEEE Transactions on Communications*, vol. 66, no. 12, pp. 6527–6541, 2018.
- [68] J. Zeng, T. Lv, R. P. Liu, X. Su, Y. J. Guo, and N. C. Beaulieu, "Enabling ultrareliable and low-latency communications under shadow fading by massive MU-MIMO," *IEEE Internet of Things Journal*, vol. 7, no. 1, pp. 234–246, 2020.
- [69] H. Ren, C. Pan, K. Wang, Y. Deng, M. ElKashlan, and A. Nallanathan, "Achievable data rate for URLLC-enabled UAV systems with 3-D channel model," *IEEE Wireless Communications Letters*, vol. 8, no. 6, pp. 1587–1590, 2019.
- [70] A. Ranjha and G. Kaddoum, "Ullc facilitated by mobile UAV relay and RIS: A joint design of passive beamforming, blocklength and UAV positioning," *IEEE Internet of Things Journal*, pp. 1–1, 2020.
- [71] W. R. Ghanem, V. Jamali, and R. Schober, "Joint beamforming and phase shift optimization for multicell IRS-aided OFDMA-URLLC systems." [Online]. Available: <https://arxiv.org/abs/2010.07698>
- [72] C. Shannon, "A mathematical theory of communication," *The Bell System Technical Journal*, vol. 27, no. 1, pp. 379–423, July 1948.
- [73] H. Ren, C. Pan, Y. Deng, M. ElKashlan, and A. Nallanathan, "Joint power and blocklength optimization for URLLC in a factory automation scenario," *IEEE Transactions on Wireless Communications*, vol. 19, no. 3, pp. 1786–1801, 2020.
- [74] —, "Joint pilot and payload power allocation for massive-MIMO-enabled URLLC IIoT networks," *IEEE Journal on Selected Areas in Communications*, vol. 38, no. 5, pp. 816–830, 2020.
- [75] H. Liu, H. Ding, L. Xiang, J. Yuan, and L. Zheng, "Outage and BER performance analysis of cascade channel in relay networks." in *FNC/MobiSPC*, 2014, pp. 23–30.

- [76] I. S. Gradshteyn and I. M. Ryzhik, *Table of integrals, series, and products*. Academic press, 2014.
- [77] Wolfram Research, Inc., “Mathematica, Version 11.0.” [Online]. Available: <https://www.wolfram.com/mathematica>
- [78] Wolfram, “Polygamma function.” [Online]. Available: <https://reference.wolfram.com/language/ref/PolyGamma.html>
- [79] —, “Eulergamma.” [Online]. Available: <https://reference.wolfram.com/language/ref/EulerGamma.html>
- [80] Wikipedia, “Polygamma approximation.” [Online]. Available: <https://en.wikipedia.org/wiki/Polygamma-function>